MLC30: A New 30 m Land Cover Dataset for Myanmar From 1990 to 2020 Using Training Sample Migration Framework

Huaqiao Xing, Linye Zhu, Yuqing Zhang, Dongyang Hou, *Member, IEEE*, and Cansong Li

***Abstract*—Myanmar has experienced rapid socio-economic developments in recent decades, which have a greater impact on land cover change. Accurate long time series land cover datasets for Myanmar can be of great help in environmental protection and natural resource management. However, there are relatively few existing studies on long time series land cover datasets in Myanmar, and the acquisition of training samples within different time series is a big challenge. Therefore, this study used Google Earth Engine and Landsat imagery to produce a land cover dataset for every two years from 1990 to 2020 using a training sample migration framework. First, the differences in index change, spectral value change, and spectral shape change were used to determine whether the sample points had changed between the base year and the previous year, and then a small number of samples were manually selected. Second, the spectral features, index information, and texture information of the remote sensing images and the object-oriented segmentation method were used to obtain object-oriented multidimensional features. Finally, the random forest method was employed to train the samples of the previous year to obtain the land cover data of the previous year. The results of the study show that the average overall precision of the land cover classification results for Myanmar for 1990–2020 is 0.83 and Kappa is 0.79. In addition, the land cover classification results for Myanmar of 1990–2020 are significantly better than those of Globeland30-2020, FROM-GLC, and Dynamic World land cover, and comparing with these products showed good agreement.**

***Index Terms*—Land cover classification, Myanmar, random forest, sample migration, time series.**

Manuscript received 8 July 2023; revised 29 August 2023 and 8 October 2023; accepted 24 October 2023. Date of publication 30 October 2023; date of current version 23 November 2023. This work was supported in part by the Shandong Provincial Natural Science Foundation under Grant ZR2022YQ36, in part by the Youth Innovation Team Project of Higher School in Shandong Province under Grant 2022KJ201, in part by the Science and Technology Basic Resources Survey of China under Grant 2019FY202503, and in part by the Yunnan Provincial Philosophy and Social Science Innovation Team Construction Project under Grant 2023CX02. *(Corresponding authors: Dongyang Hou; Cansong Li.)*

Huaqiao Xing and Yuqing Zhang are with the School of Surveying and Geo-Informatics, Shandong Jianzhu University, Jinan 250101, China (e-mail: xinghuaqiao18@sdjzu.edu.cn; 2022160103@stu.sdjzu.edu.cn).

Linye Zhu is with the College of Geoscience and Surveying Engineering, China University of Mining and Technology, Beijing 100083, China (e-mail: bqt2200205059@student.cumtb.edu.cn).

Dongyang Hou is with the School of Geosciences and Info Physics, Central South University, Changsha 410083, China (e-mail: houdongyang1986@cumt.edu.cn).

Cansong Li is with the Faculty of Geography, Yunnan Normal University, Kunming 650092, China (e-mail: cansongli@126.com).

Digital Object Identifier 10.1109/JSTARS.2023.3328309

I. Introduction

LAND cover is the distribution of different feature types (e.g., forest, grassland, cultivated land, water bodies) on the surface of the Earth within a given area [1], [2]. Land cover has important implications for ecosystem function, climate change, the water cycle, biodiversity, and human activities.

Advancements in satellite exploration technology have enabled the collection of vast amounts of Earth observation data, which serve as a foundation for creating accurate and long-term training land cover data. For instance, Hansen et al. [4] developed global land cover datasets with a resolution of 1 km for the year 1998 [3]. Loveland et al. [5] provided global land cover data for the years 1992–1993 at resolutions of 0.25°, 0.5°, and 1° [6]. Sulla-Menashe et al. [7] provided annual global land cover datasets with a resolution of 500 m for 2001–2016 [8]. Li et al. [9] provided global land cover data with a resolution of 300 m from 1992 to 2015 based on the Food and Agriculture Organization of the United Nations land cover classification system [10]. Liu et al. [11] published a 34-year-long comprehensive record of global land cover dynamics from 1982 to 2015 at a resolution of 5 km. However, the coarse resolution of these land cover datasets makes it difficult to observe the spatial and temporal distribution of land cover and its dynamics at a finer scale.

In recent years, there has been an increase in the publication of high-resolution land cover data by research scholars [12], [13]. For example, Chen et al. [14] released more than 30 types of global land cover data browsing services (GlobeLand30) for cultivated land, artificial surfaces, water bodies, and grassland for the years 2000, 2010, and 2020, along with data download services. Gong et al. [15] released fine-resolution data for global land cover products at resolutions of 10 m and 30 m for the years 2010, 2015, and 2017 [16]. Zhang et al. [17] made available to the public the global 30 m land cover fine-resolution classification products for the years 2015 and 2020. Liu et al. [18] published high-resolution data mapping of dynamic changes in urban land use for a global continuous time period from 1985 to 2015, with a resolution of 30 m. ESRI has released global land cover data at a resolution of 10 m for 2020 to the public. Brown et al. [19] have used 10 m Sentinel-2 data coupled with deep learning methods to create Dynamic World, which is a globally consistent, high-resolution, near real-time land-use land cover classification product. In addition, Xian et al. [20]

have developed the Land Change Monitoring, Assessment, and Projection dataset, which includes annual land cover and land cover change products for the period 1985–2017 at a resolution of 30 m. Boston University team released the Global Land Cover Estimates, which are annual maps of global land cover at a resolution of 30 m from 2001 to 2020. Google team released Dynamic World, a near real-time global land use cover data at 10 m resolution that has been continuously updated on Google Earth Engine (GEE) since 2015. However, due to the large workload and relatively long time interval of the above land cover datasets, it may not always be feasible to obtain data from these sources at frequent intervals.

In addition, supervised machine learning methods are a common tool in constructing land cover data. Regardless of which supervised machine learning method is utilized to obtain land cover data, the number and the quality of training samples are important factors in determining the accuracy of the land cover data. The accurate acquisition of long training samples is still a problem to be solved. For example, Ghorbanian et al. [21] used Sentinel-1 and Sentinel-2 data to compare spectral differences through the spectral angle distance (SAD) method to migrate the 2017 sample to 2019 to obtain land cover classification results. Huang et al. [22] used Landsat data to compare spectral differences by the SAD method and the Euclidean distance method to obtain land cover classification results for five target years. However, the above-mentioned method only considers spectra in terms of the difference between the spectra of the base and reference years, which may impact the accuracy of the training samples. Therefore, there is a need to obtain classification results from a more comprehensive perspective of carving out the changes.

Myanmar is a country with vast stretches of land and abundant natural resources, including diverse forests, rivers, and wildlife [23], [24]. Given its strategic position in Southeast Asia and significant geopolitical and economic value, Myanmar holds immense importance from a global perspective. Despite this, Myanmar remains an underdeveloped country, and relatively little research has been conducted on its long-term land cover trends. Therefore, studying land cover change in Myanmar and conserving its natural resources and cultural heritage could improve the living conditions and economic opportunities for local communities and contribute to the preservation and development of global ecosystems and cultural diversity [25], [26]. By understanding the dynamics of land cover change and promoting sustainable land use practices, Myanmar can ensure the long-term health and well-being of its people and environment while contributing to the conservation of biodiversity and cultural heritage globally.

This study aims to examine the changes in land cover in Myanmar over a 30-year period from 1990 to 2020 using a training sample migration framework. To achieve this goal, GEE and Landsat remote sensing images were utilized to create land cover data every two years. First, base year samples were selected based on GlobeLand30 data and high-resolution images. Differences in index changes, spectral value changes, and spectral shape changes were used to determine whether the sample points changed between the base year and the previous year. A portion of the sample points were then selected by manual visual interpretation to supplement the sample points lost due to sample migration to obtain sample points from previous years. Second, the spectral features, index information, and texture information of the remote sensing images were analyzed in combination with object-oriented segmentation methods in order to obtain the multidimensional features of the images. Finally, the previous year's samples were used in combination with the random forest method to obtain the previous year's land cover classification results.

The main contribution and innovation of our work is the creation of a comprehensive 30 m land cover dataset for Myanmar land cover every two years from 1990 to 2020 (MLC30) using a training sample migration framework. We achieved sample point migration by examining index differences, spectral values, and spectral shapes, which reduced the manual selection workload. In addition, we utilized multidimensional remote sensing image features combined with object-oriented segmentation methods, resulting in improved accuracy and completeness of the land cover classification results. This dataset is crucial in facilitating spatial planning and monitoring of land cover dynamics in Myanmar.

The rest of the article is organized as follows. Section II describes the study area and the data used. Section III provides an introduction to the method of construction of the dataset. Section IV presents the corresponding analysis of the dataset. Conclusions and future work are given in Section V.

II. Study Area and Data

A. Study Area

As shown in Fig. 1, Myanmar is situated in the northwestern region of the South-Central Asian peninsula. It is bordered by latitude 8°49'–28°32'N and longitude 92°10'–101°10'E. The country's topography features lofty mountains in the north and low-lying plains in the south, with surrounding mountain ranges embracing the east, north, and west regions [27]. Myanmar is administratively divided into seven regions, seven states, and two central municipalities, and forests cover an expansive 42.92% of its land area [28], [29].

B. Data

The Landsat series of satellites is widely considered to be an optimal data source for high-resolution and large-scale land cover monitoring. In this study, the Landsat series data were obtained through the GEE cloud computing platform [30], [31]. The images for each year were composited using a cloud mask, which removed pixels with high cloud cover, resulting in the median of the annual Landsat observation series for that year. The Myanmar Long Time Series Land Cover Classification product spans from 1990 to 2020 and consists of 16 issues produced every two years. The data utilized Landsat 5 images for the years 1990, 1992, 1994, 1996, 1998, 2000, 2002, 2004, 2006, 2008, and 2010; Landsat 7 images in 2012; and Landsat 8 images in 2014, 2016, 2018, and 2020.

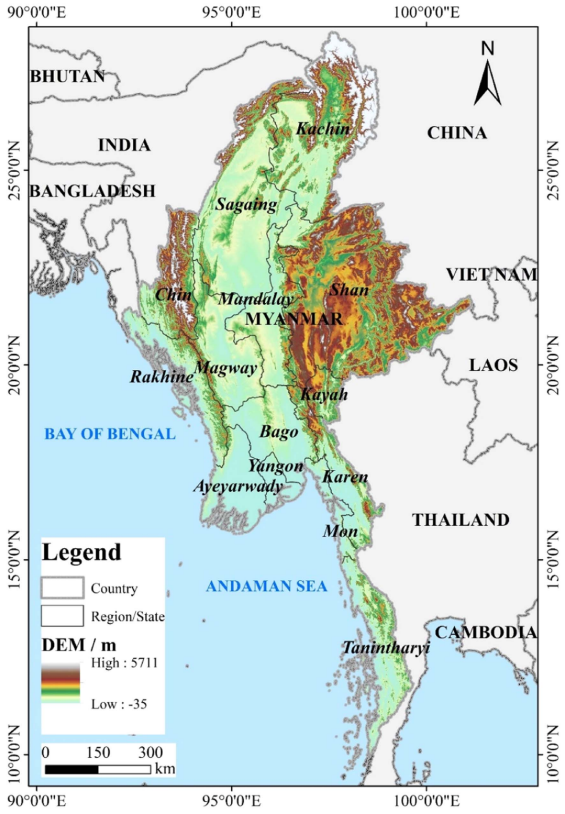

Fig. 1. Spatial location of the study area.

To ensure the accuracy of the migration sample, this study utilized high-resolution remote sensing imagery and the GlobeLand30 global land cover products for the years 2000, 2010, and 2020 [32]. The GlobeLand30 product has undergone extensive third-party accuracy evaluations, which resulted in an overall accuracy (OA) of 83.50% and a Kappa coefficient of 0.78 for its 2010 version [33]. The GlobeLand30 products classify land cover types into cultivated land, forest, grassland, shrubland, wetland, water bodies, artificial surfaces, bare land, and permanent snow and ice. As shown in Fig. 2, the number of samples of different types fluctuates to varying degrees from year to year.

III. Methodology

The training sample migration framework is shown in Fig. 3.

1) Migration of sample points based on index and spectral The index difference change and the spectral value and spectral shape difference change between the base year and the previous year's image were used to determine whether the base year sample had changed in the previous year. A small number of samples were manually selected to obtain the previous year's samples, thus obtaining the previous year's land cover classification results.
2) Acquisition of multidimensional features from remote sensing images The spectral features of the intrayear time series remote sensing images were used to calculate the corresponding index information and texture features, combined with the simple noniterative clustering (SNIC) method to obtain object-oriented multidimensional features.
3) Acquisition of classification results based on the random forest Using a combination of Globeland30 data and high-resolution imagery, the samples of the base year were selected to obtain the land cover classification results by the random forest method.

A. Migration of Sample Points Based on Index and Spectral

The remote sensing images of the base year and the previous year are tested for changes in order to obtain a sample suitable for the previous year based on the sample of the base year. By comparing the degree of difference in index, the degree of difference in spectral value, and the degree of difference in spectral shape between the remote sensing image of the base year and the remote sensing image of the previous year, it is determined whether the sample area of the base year and the previous year has changed. In this regard, the degree of difference in indices is calculated using absolute distances, while the degree of difference in spectral magnitudes and the degree of difference in spectral shapes are calculated by the change vector analysis (CVA) [34], [35] and spectral angle mapper (SAM) methods, respectively. On this basis, the OTSU method is used to determine whether the corresponding sample point has changed.

When no change was detected in the change in index difference, spectral value difference, and spectral angle difference between the base year and the previous year's remote sensing image, the sample points were retained as the previous year's sample points. A small number of samples are further hand-selected to obtain the previous year's land cover classification results by the random forest method. The specific formula is as follows:

$$\sum_{i=1}^{n} \left| x_{a_{\text{index}}} - x_{b_{\text{index}}} \right| \tag{1}$$

$$\text{CVA} = \sqrt{\sum\nolimits_{i=1}^{n} \left(x_{a_i} - x_{b_i} \right)^2} \tag{2}$$

$$\text{SAM} = \arccos \times \left(\frac{\sum_{i=1}^{n} (x_{a_i} - \overline{x_a}) \times (x_{b_i} - \overline{x_b})}{\sqrt{\sum_{i=1}^{n} (x_{a_i} - \overline{x_a})^2 \times \sum_{i=1}^{n} (x_{b_i} - \overline{x_b})^2}} \right) \tag{3}$$

where x_{a_i} and x_{b_i} are the spectral values of remote sensing images in the base year and the previous year, respectively. $\overline{x_a}$ and $\overline{x_b}$ are the mean of the spectral values from remote sensing images in the base year and the previous year, respectively. i is the corresponding bands of the base year and the previous year. index is the normalized difference vegetation index (NDVI), normalized difference water index (NDWI), and normalized difference built-up index (NDBI), respectively.

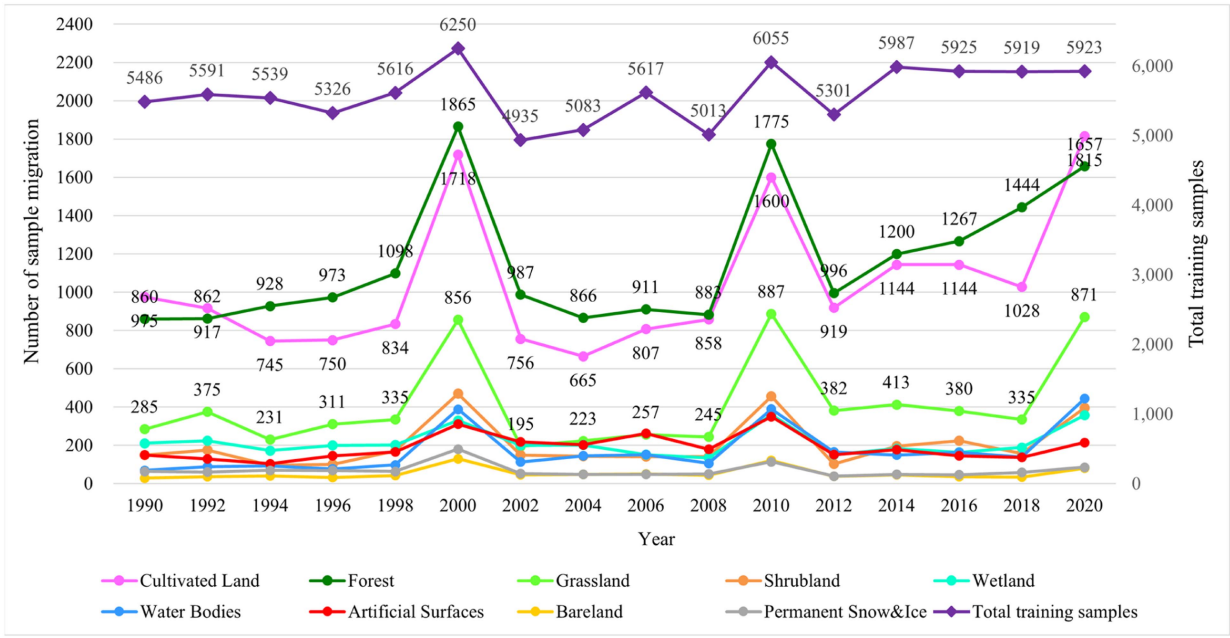

Fig. 2. Sample numbers of migrations in different years.

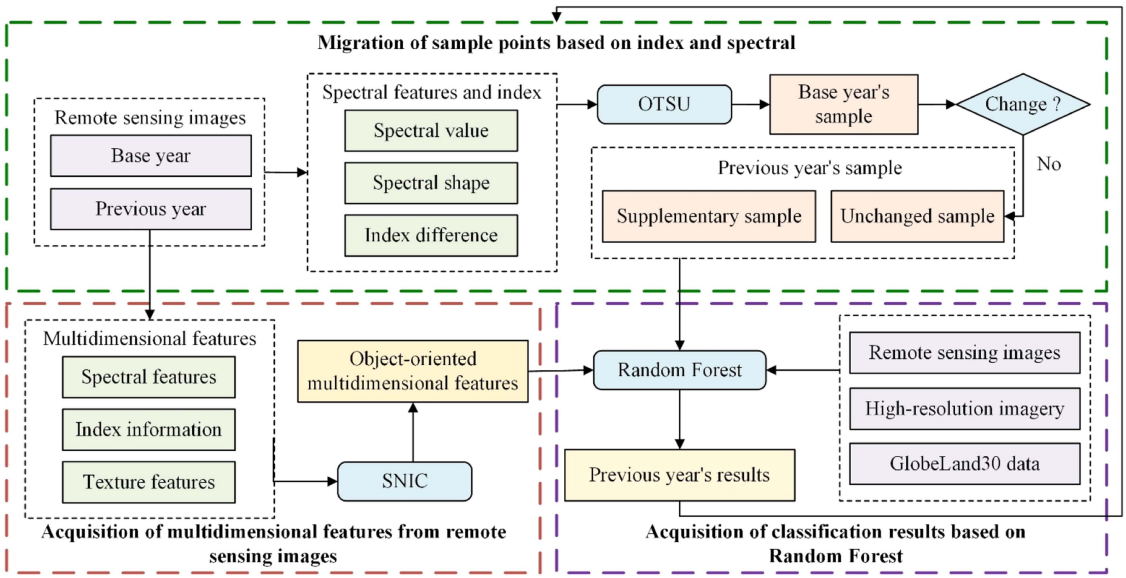

Fig. 3. Flowchart of the training sample migration framework. Migration of sample points based on index and spectral; acquisition of multidimensional features from remote sensing images; acquisition of classification results based on the random forest.

As shown in Fig. 4, pixel points A and B did not change in years T1 and T2. Pixel A was not detected as a change in the NDVI change results, NDWI change results, NDBI change results, spectral value change results, and spectral shape change results. Thus, we consider pixel A to be an unchanged point that can be used as a migration sample. Pixel point B was detected as a change in the spectral value change but was otherwise not detected as a change. In this case, we exclude pixel B as a sample that can be migrated to avoid pseudochange due to extraneous factors and ensure that the migrated sample is as much as possible an area that has not changed to obtain an accurate land cover type.

B. Acquisition of Multidimensional Features From Remote Sensing Images

To avoid cloud and cloud shadow occlusion and vegetation phenological growth, the remote sensing images were composited for January–February, March–September, and October–December during the year. Different spectral indexes can express

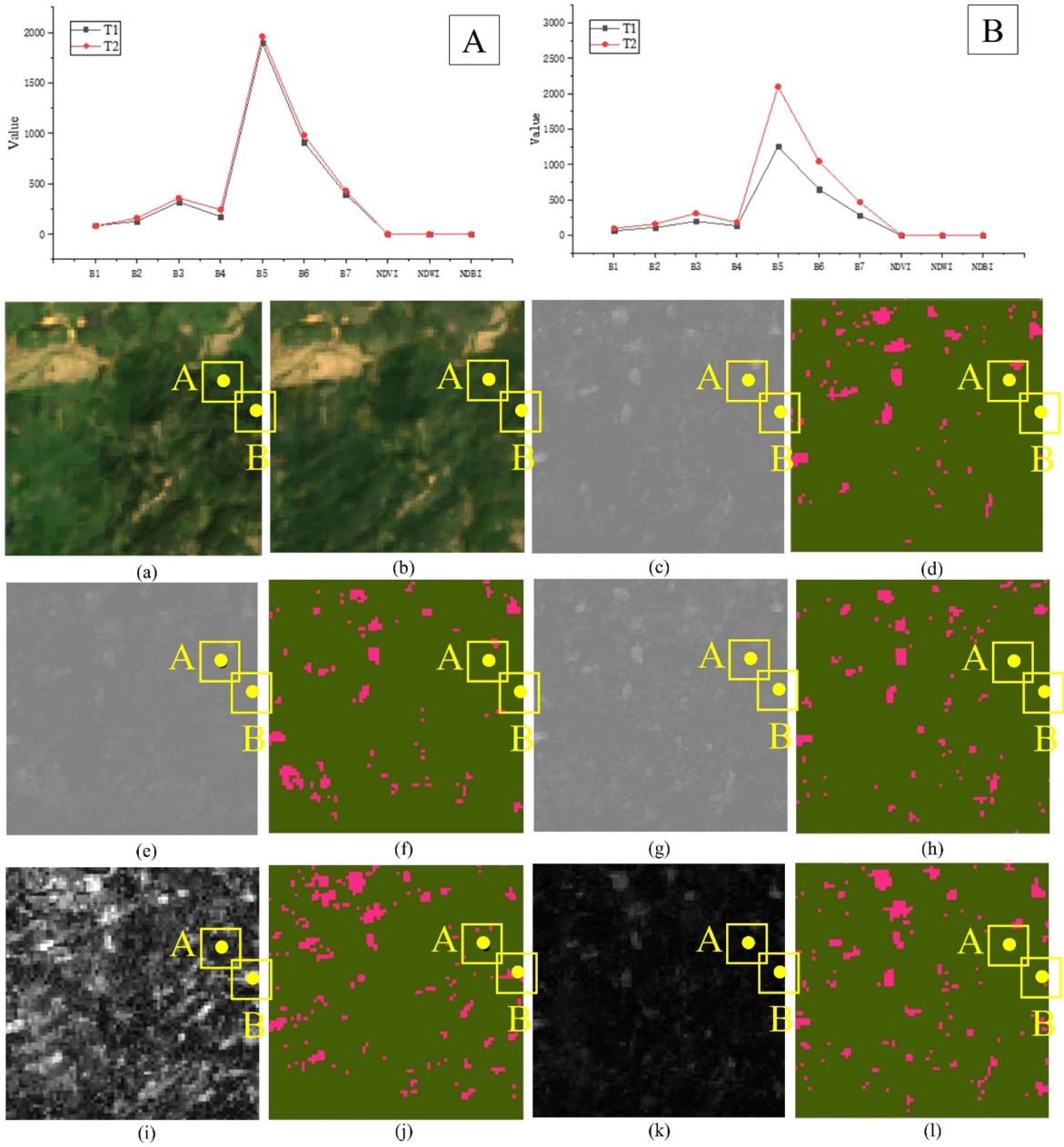

Fig. 4. Spectral curves of pixel A and pixel B and the change detection results under different feature information. (a) T1. (b) T2. (c) NDVI differences. (d) NDVI changes. (e) NDWI differences. (f) NDWI changes. (g) NDBI differences. (h) NDBI changes. (i) Spectral value differences. (j) Spectral value changes. (k) Spectral shape differences. (l) Spectral shape changes.

the characteristic information of different land cover types to different degrees. NDVI is a commonly used index for measuring the extent and growth of vegetation cover and can provide important information on the distribution and change of surface vegetation. NDWI is an index used to extract information about water bodies and can be used to distinguish between water bodies and nonwater bodies. NDBI is an index for extracting information on buildings for accurate judgment of building distribution and density. Enhanced vegetation index (EVI) is a vegetation index that improves on NDVI by introducing atmospheric correction factors and soil conditioning factors, which can more accurately reflect the growth status and degree of vegetation cover. Ratio vegetation index (RVI) is an index that measures the extent of vegetation cover and provides information on the distribution and condition of vegetation. NDVI, NDWI, NDBI, EVI, and RVI are calculated using remote sensing images. Multidimensional features of remote sensing images are constructed using remote sensing image bands 1–7, index information, and the corresponding gray-level cooccurrence matrix (GLCM) texture features (i.e., contrast, entropy, correlation, and dissimilarity). The specific equations are as follows:

$$\mathrm{NDVI} = \frac{\rho_{\mathrm{nir}} - \rho_{\mathrm{red}}}{\rho_{\mathrm{nir}} + \rho_{\mathrm{red}}} \tag{4}$$

$$\mathrm{NDWI} = \frac{\rho_{\mathrm{green}} - \rho_{\mathrm{nir}}}{\rho_{\mathrm{green}} + \rho_{\mathrm{nir}}} \tag{5}$$

$$\mathrm{NDBI} = \frac{\rho_{\mathrm{swir}} - \rho_{\mathrm{nir}}}{\rho_{\mathrm{swir}} + \rho_{\mathrm{nir}}} \tag{6}$$

$$\mathrm{RVI} = \frac{\rho_{\mathrm{nir}}}{\rho_{\mathrm{red}}} \tag{7}$$

$$\mathrm{EVI} = 2.5 \times \frac{\rho_{\mathrm{nir}} - \rho_{\mathrm{red}}}{\rho_{\mathrm{nir}} + 6\rho_{\mathrm{red}} - 7.5\rho_{\mathrm{blue}} + 1} \tag{8}$$

where ρ_{red}, ρ_{green}, ρ_{blue}, ρ_{nir}, and ρ_{swir} are the red, green, blue, near-infrared, and short-wave infrared bands, respectively.

GLCM [36] is a commonly used method for extracting texture features from images. This technique involves calculating the probability of a specific grayscale value appearing at a fixed distance and direction from a given pixel with a grayscale value [37]. The results are represented in the form of a matrix. To extract texture features corresponding to spectral bands and indexes, commonly used statistics such as contrast, entropy, correlation, and dissimilarity were selected.

On this basis, the SNIC method is used for object-oriented segmentation of multidimensional features in remote sensing images. This helps to reduce the "salt and pepper" phenomenon that can occur in classification results. The SNIC algorithm is a noniterative superpixel-based clustering algorithm that is primarily used for image segmentation. Traditional image segmentation methods often require manual selection of thresholds or iterative clustering based on image features, which can be challenging to achieve optimal segmentation results for different scenes and images [38]. However, the SNIC algorithm improves the segmentation outcome by dividing the image into multiple local regions known as superpixels. These superpixels are generated using weights for spatial distance and color similarity, hence preserving image detail information. Moreover, the size and number of superpixels can be adaptively adjusted by the SNIC algorithm leading to more accurate image segmentation [39], [40].

C. Acquisition of Classification Results Based on the Random Forest

This study utilizes Globeland30 data and high-resolution images to select 4000–6000 training samples for the base years of 2000, 2010, and 2020. For each year, 70% of the sample points are randomly selected as training samples and the remaining 30% serve as test samples. Random forest is then employed to obtain land cover classification results. The random forest method is a combined classifier comprising classification and regression trees (CART) [41]. Each CART is trained using the Bootstrapping method to create a training set. In addition, the random subspace method is introduced during training to improve the classification accuracy of the CART tree [42]. Unknown samples are classified using majority voting. As an integrated learning algorithm, random forest is an extended variant of Bagging integrated learning that uses CART as the base learning algorithm [43]. The convergence of random forest is similar to Bagging in that individual learners' generalization performance and robustness in random forest are poor when only one learner is included. However, as the number of individual learners increases, the generalization error of the random forest converges to a minimum. During training, random forest can estimate the importance of feature variables, which makes it more adaptive and able to maintain accuracy even if there is missing data in the classification process. The random forest out-of-bag estimation method provides an unbiased estimate of the generalization error, ensuring that the model can generalize well. The random forest model parameters are set as follows. The number of trees is 1000, other parameters are set to default settings, the variables per split is null, minleaf population is 1, bag fraction is 0.5, maxnodes is null, and seed is 0.

IV. Results and Discussion

A. Data Accuracy and Comparison With Other Datasets

The accuracy of the MLC30 product was evaluated based on the validation sample, with the OA, Kappa coefficient, F1-score, specificity, producer accuracy (PA), and user accuracy (UA). As shown in Fig. 5, the results indicate that the OA of the MLC30 product is 0.83, the Kappa coefficient is 0.79, the specificity is 0.94, and the F1-score is 0.78. Overall, the base years 2000, 2010, and 2020 have the highest accuracy, with OA, Kappa coefficient, and F1-score all reaching above 0.85, and specificity reaching above 0.95. The years 1990–2006 have a lower accuracy with the OA around 0.78, Kappa coefficient around 0.73, specificity around 0.93, and F1-score around 0.70. Years 2008–2020 had higher accuracy, with OA around 0.87, Kappa coefficient around 0.82, specificity around 0.95, and F1-score around 0.83. In terms of individual categories, forests have the best classification accuracy, with UA and PA of 0.85 and 0.94, respectively. Wetlands have the second-highest accuracy, with UA and PA of 0.91 and 0.86, respectively. Grassland, shrubland, and bare land have relatively low accuracy, with a PA of no more than 0.7. This is because, in reality, these three land types are often intermixed and, therefore, more difficult to categorize. The UA and PA of water bodies and permanent snow and ice have smaller differences, with 0.89 and 0.86 for water bodies and 0.81 and 0.83 for permanent snow and ice, indicating that they are not easy to be confused with other land types and their classification accuracy is more stable. Overall, the accuracy of the MLC30 product is satisfactory and the reliability is high.

To better reflect the quality of the MLC30 product, the 2020 MLC30 was compared with the 2020 Globeland30, FROM-GLC, and Dynamic World land cover products, as shown in Fig. 6. In terms of OA, MLC2020 shows a significant improvement over GlobeLand30, FROM-GLC, and Dynamic World. In terms of the Kappa coefficient, MLC2020 was the highest at 0.86, indicating that MLC2020 showed better ability in terms of accuracy and consistency of the overall classification results. For the F1-score, the F1-score of MLC2020 is 0.86, which is higher than the 0.82, 0.82, and 0.75 of the other three products, indicating that the comprehensive accuracy of the classification results of MLC2020 is excellent. Also, MLC2020's specificity stands out over the other three categories at 0.96. In several land classes, MLC2020 shows higher classification accuracy than the other three products. For example, for cultivated lands, forests,

Fig. 5. Results of the evaluation of the accuracy of land cover products in Myanmar, 1990–2020.

wetlands, water bodies, artificial surfaces, and permanent snow and ice, MLC2020 has a higher PA than the other three products, and for grasslands and shrublands, it is only lower than GlobeLand30. For forest, grassland, shrubland, wetland, bare land, artificial surfaces, and permanent snow and ice, MLC2020 has a higher UA than the other three products.

As shown in Fig. 7, to further explore the differences between MLC30 and GlobeLand30, Dynamic World, and GLC-FCS30, the four sets of products were compared in local areas. MLC30 showed similar results to other datasets for artificial surfaces, while for forests it was similar to GlobeLand30 and Dynamic World in Region A. For water bodies, MLC30's classification closely resembled that of Dynamic World. MLC30 was more accurate in distinguishing between cultivated land, grassland, and shrubland than Dynamic World. In Region B, MLC30 outperformed GLC-FCS30 in differentiating between forest and shrubland. Although the forest distribution in MLC30 is similar to that of GlobeLand30 and GLC-FCS30, this dataset is more effective in identifying scattered and fragmented vegetation within cultivated land. In Region G, MLC30 showed a similar distribution of wetlands as GlobeLand30 and GLC-FCS30. However, MLC30 was more accurate in distinguishing wetlands from forests and could extract water bodies more completely compared to the other two datasets.

B. *Land Cover Classification Results*

Fig. 8 shows land cover data for Myanmar from 1990 to 2020. It is remarkable to see the spatial differentiation of land cover in Myanmar, with each region having its unique characteristics and distribution of land cover types. The eastern Shan Plateau is dominated by forests, cultivated lands, grasslands and shrublands, while the Naga Hills and Rakhine Mountains are mainly forest and grassland. Coastal areas have cultivated land and wetlands, and the Ayeyarwady delta is dominated by cultivated land, wetlands, and artificial surfaces. The remaining Himalayan ranges in the north are covered by forests, and the central mid-Ayeyarwady valley is dominated by cultivated land and artificial surfaces.

Another interesting observation is that Myanmar's water bodies are predominantly rivers, which are distributed along the Ayeyarwady system, including the Nmai Hka River and Mali River in the upper reaches and the Chindwin River in the middle reaches and the Salween River system and the Sittang River.

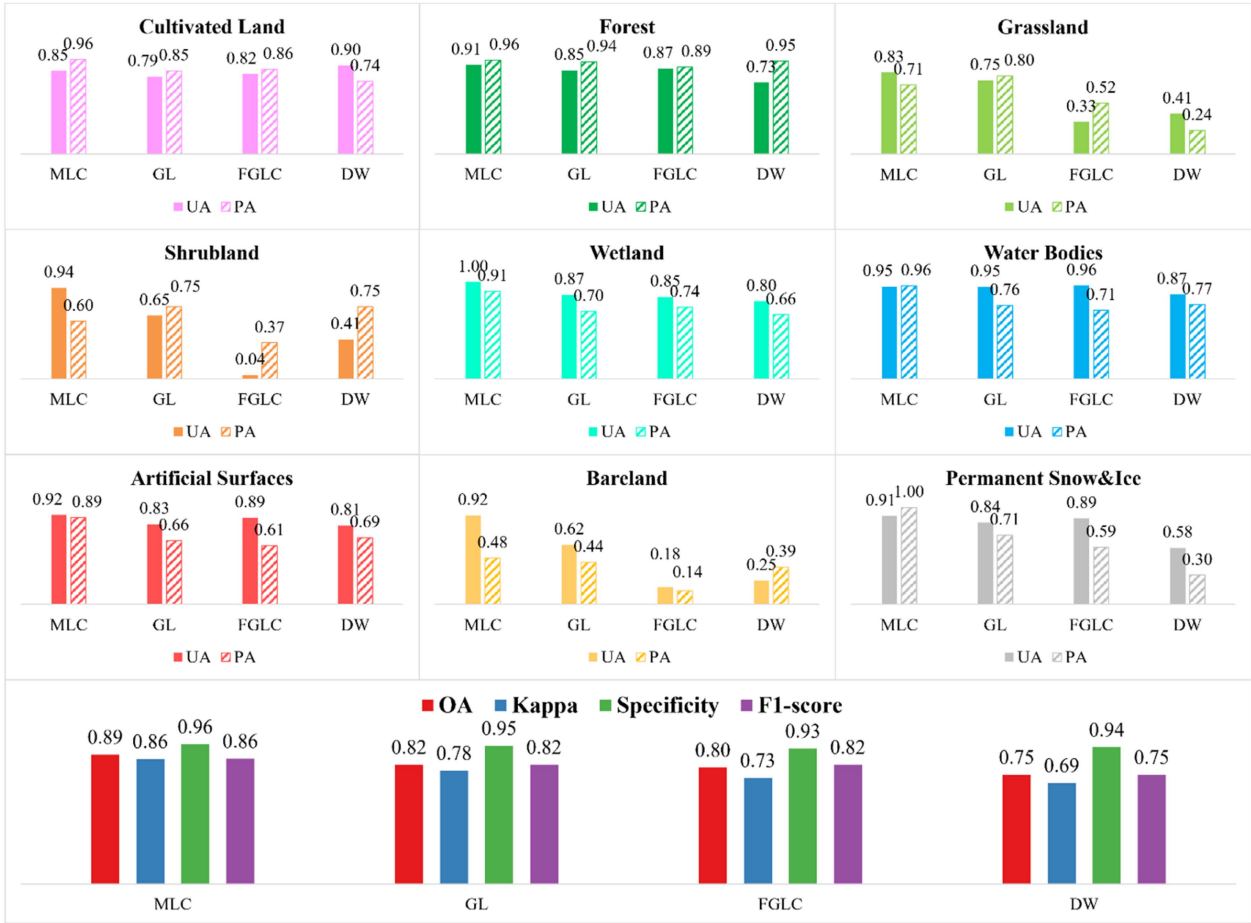

Fig. 6. Comparison of accuracy evaluation results for MLC2020, GlobeLand30, FROM-GLC, and dynamic world in 2020.

Most of Myanmar's water bodies are distributed along these three major water systems. This information can be valuable for planning and management purposes, such as identifying areas that require conservation or restoration efforts, assessing the impacts of human activities on the environment, and planning infrastructure development in a sustainable manner.

From the 1990–2020 classification results, the land categories with high overall consistency are cultivated land, forests, water bodies, wetlands, and artificial surfaces. Cultivated land and forests, although misclassified to a certain extent every year, have a huge total area and have less impact on their overall consistency. Although there is a gradual decrease in the area of wetlands and a gradual increase in the area of water bodies and artificial surfaces, the spatial distribution of the three is stable. The land categories with low overall consistency are grassland, shrubland, bare land, and permanent snow and ice. Grasslands and shrublands are easily misclassified with cultivated land and forests, and their total area is not large enough, so their spatial distribution and area fluctuate considerably. Although the spatial distribution of bare land and permanent snow and ice is more stable, the area of both fluctuates more with climate change. Regionally, areas with high taxonomic consistency are mainly in areas with high forest cover, such as Sagaing, Kachin, Tanintharyi, Chin, and Rakhine. These areas are mostly mountainous and economically backward, with very limited human activities and low land cover change. Areas with lower taxonomic consistency are concentrated in the center and south, such as Magway, Mandalay, Yangon, and Ayeyarwady. These areas are lower in elevation, mostly plains, more economically developed, and densely populated, and have a greater demand for land, with greater variations in land types such as artificial surfaces, cultivated land, and grasslands.

Fig. 9 and Table I illustrate that the spatial distribution of land cover patterns in Myanmar closely resembles the actual situation, providing an accurate reflection of the country's land cover. The majority of forests are concentrated in the northern, eastern, and western regions, with cultivated land and artificial surfaces more prevalent in the central and southern areas. Analysis of the 2020 MLC30 data reveals that forests, grasslands, and shrublands are predominantly located in the north, particularly in the Shan Plateau, Naga Hills, Rakhine Mountains, and the remainder of the Himalayas. Notably, Shan State, Kachin State, and Sagaing account for 57.24% of the total forests, while only 3.57% is found in Mon State, Ayeyarwady, and Yangon. Grasslands and shrublands are mainly concentrated in Shan State and Magway, as shown in Fig. 9(d) and (f), accounting for 52.39% and 56.11% of the total grassland and shrubland, respectively.

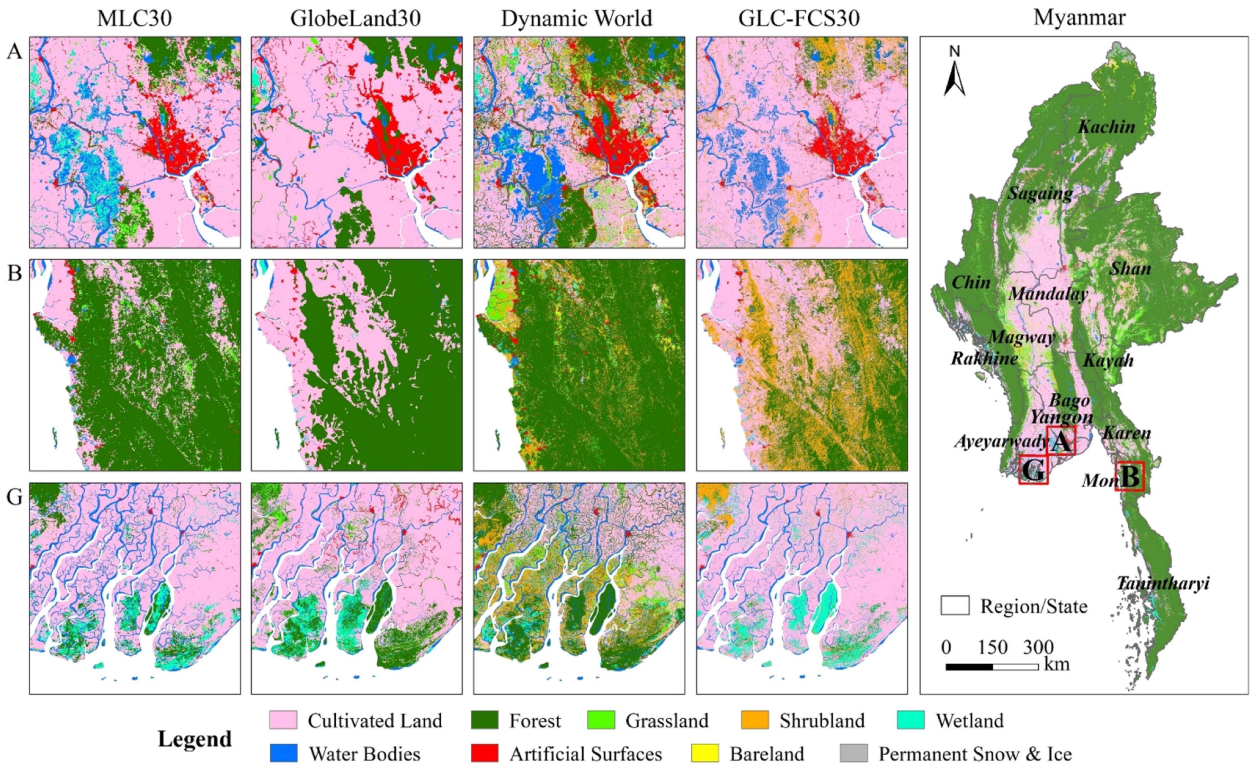

Fig. 7. Local comparison of MLC30 and other land cover datasets.

TABLE I
AREA AND PROPORTION OF LAND COVER IN MYANMAR, 1990–2020

Class\Year	Area/km^2	Percent/%	Area/km^2	Percent/%	Area/km^2	Percent/%	Area/km^2	Percent/%
	1990		2000		2010		2020	
Cultivated land	192300	26.68	188315	26.13	210368	29.19	189878	26.35
Forest	447917	62.15	463310	64.29	440302	61.09	452606	62.80
Grassland	41935	5.82	39796	5.52	33553	4.66	38049	5.28
Shrubland	11225	1.56	5480	0.76	9810	1.36	6814	0.95
Wetland	8299	1.15	6965	0.97	6772	0.94	6471	0.90
Waterbodies	8913	1.24	10886	1.51	12038	1.67	14941	2.07
Artificial surfaces	3449	0.48	3358	0.47	4908	0.68	7292	1.01
Bare land	5234	0.73	1108	0.15	1161	0.16	2508	0.35
Permanent snow and ice	1427	0.20	1481	0.21	1787	0.25	2141	0.30

In contrast to the distribution of forests, cultivated land and artificial surfaces are mostly found in the south and less commonly in the north. The central mid-Ayeyarwady valley has the highest concentration of arable land, whereas the southern Ayeyarwady delta region has the highest concentration of artificial surfaces. The majority of cultivated land is situated in Sagaing, Shan State, Magway, as shown in Fig. 9(d), Mandalay, and Ayeyarwady, constituting 72.63% of the total cultivated land area. Furthermore, central Sagaing and Mandalay account for 29.68% of the total artificial surfaces, while the Ayeyarwady, Bago, and Yangon in the Ayeyarwady Delta, as shown in Fig. 9(a), account for 37.99%. Myanmar's wetlands are primarily located in the western coastal region of Rakhine State and the Ayeyarwady Delta. Bare land and permanent snow and ice are concentrated in the northernmost part of Kachin State within the remaining Himalayan range. Roughly 80.29% of the total wetland area is situated in Rakhine State, Tanintharyi, and Ayeyarwady, as shown in Fig. 9(e). All of the permanent snow and ice and 64.48% of the bare land are located in the Remnant Himalayas, as shown in Fig. 9(c).

Fig. 10 illustrates significant changes in Myanmar's land cover from 1990 to 2020. First, the area of forest cover

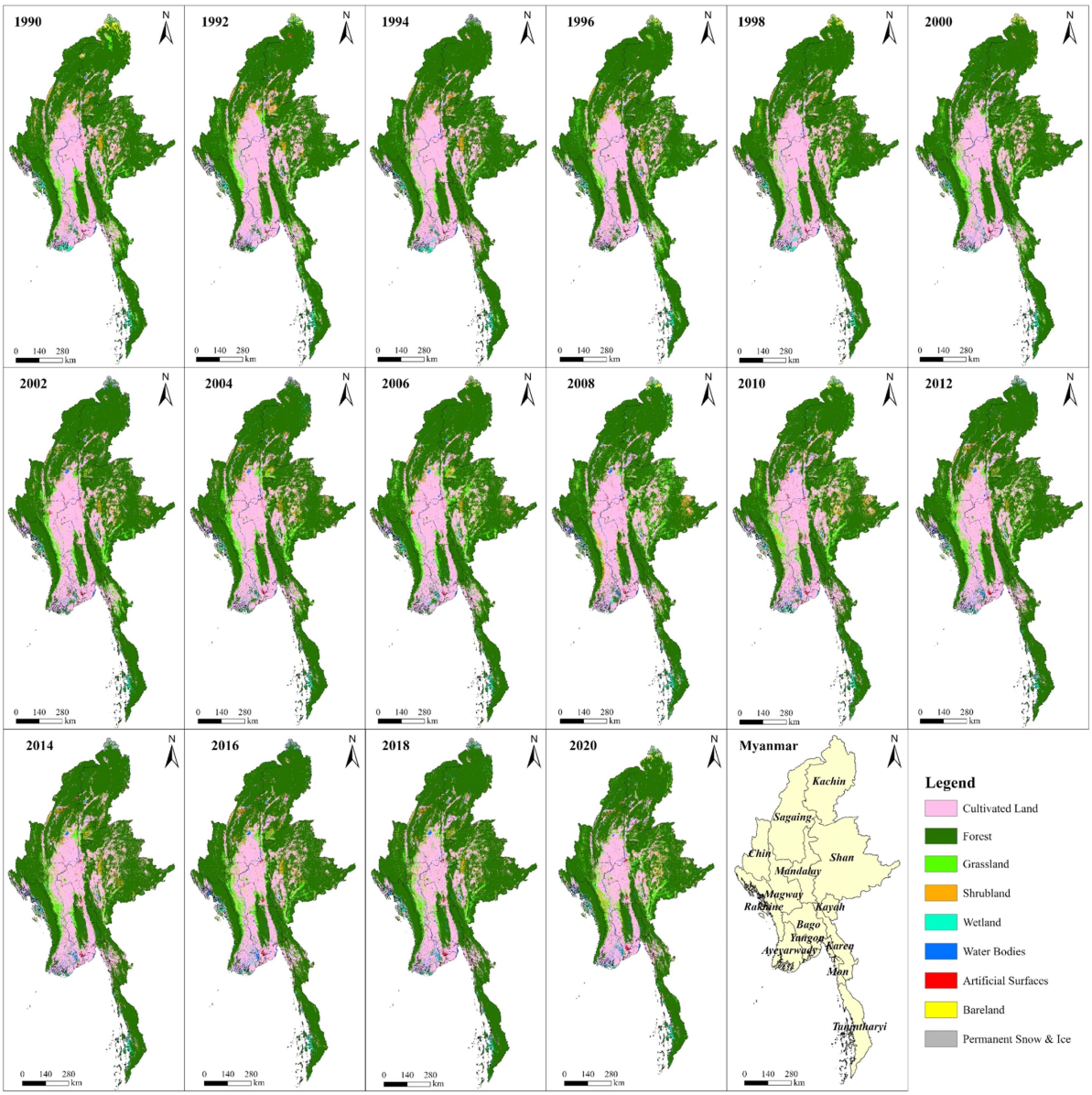

Fig. 8. Land cover map of Myanmar for 1990–2020.

experienced slight fluctuations during this period, with a small increase overall. While the increase from 447 917 km^2 in 1990 to 452 606 km^2 in 2020 is growth, the fluctuation in forest area over this period also indicates that Myanmar's forests have experienced deforestation, degradation, and restoration, which may be due to policy changes. Second, cultivated land and grassland areas both decreased but remained relatively stable. The 0.33% reduction of 2422 km^2 of cultivated land and the decline in grassland proportion from 5.82% to 5.28% are attributable to urbanization, industrial development, and agricultural policies. The decrease in shrublands and wetlands is more pronounced, with shrublands declining from 11 225 km^2 to 6814 km^2, and wetlands diminishing from 8299 km^2 to 6471 km^2. The area of water bodies has increased significantly over this period, presumably due to water management and climate change. The area of bare land and permanent snow and ice fluctuates widely.

Myanmar has witnessed various land cover changes between 1990 and 2020, influenced by human activities, climate change, and management policies. Such changes have significant implications for Myanmar's ecosystems and sustainable development, highlighting the need for further research and sound land management policies. Promoting ecological balance and sustainable development should remain a priority for Myanmar to address these challenges.

C. Land Cover Dynamics Changes

To provide a more comprehensive analysis of land cover change trends in Myanmar and to investigate the impact of human activities on these changes, this study focuses on the following regions: the regions of Myanmar in 2020, Karen State, Mon State, and Yangon.

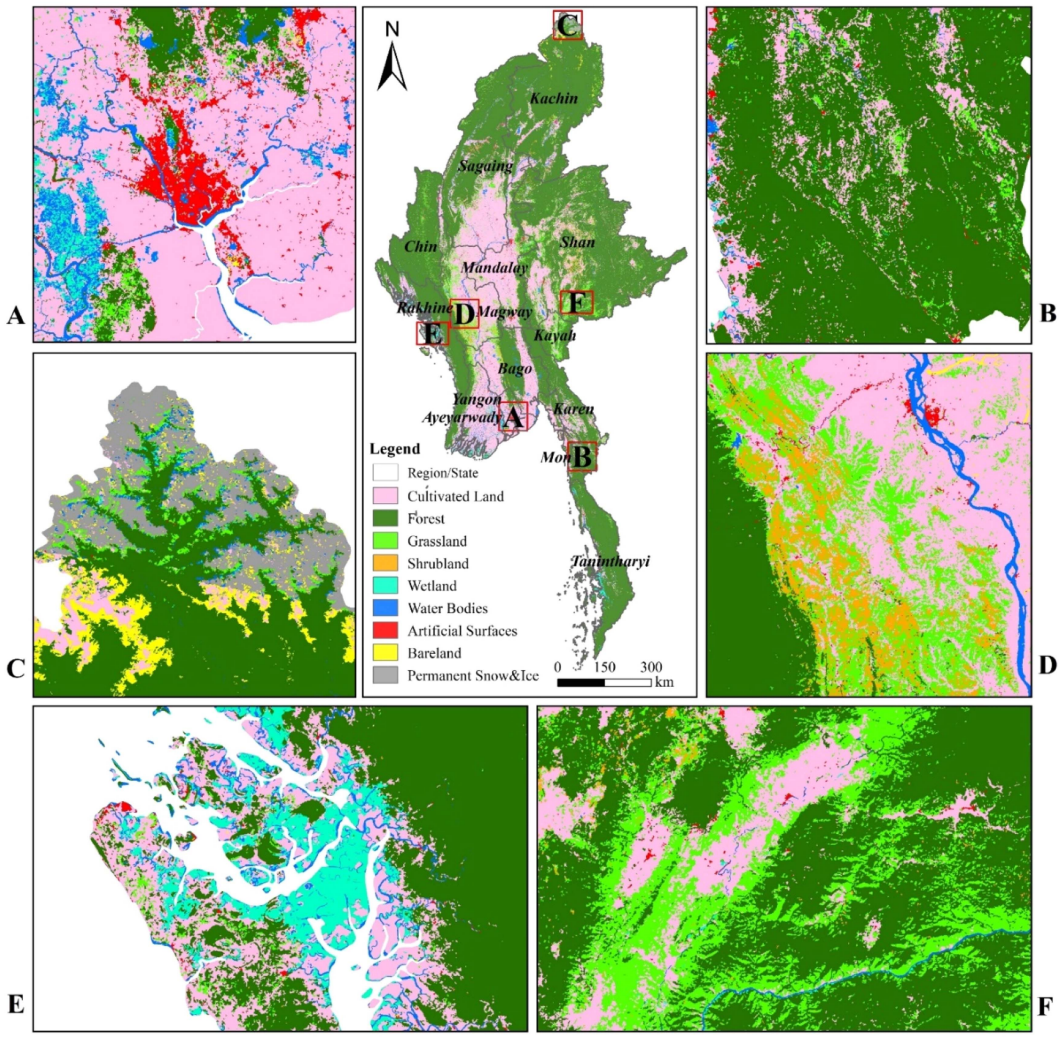

Fig. 9. Local details of land cover classification results in Myanmar in 2020.

As given in Table II, in terms of the percentage of land cover in each of the divisions of Myanmar, the situation varies considerably from one division to another, with some divisions being dominated by a particular type of land and others being more balanced. There are six divisions where the percentage of area of a single land type is more than 70%, namely, Shan, Tanintharyi, Karen, Kachin, Chin, and Rakhine. Only Bago does not have a land class with a percentage of area exceeding 50%, while the remaining seven divisions all have a single land class with a percentage of area around 60%. There are only two types of land with the highest percentage of area in the divisions: cultivated land and forests. The five divisions with the highest percentage of arable land area are Bago, Magway, Mandalay, Yangon, and Ayeyarwady, while the remaining nine divisions have the highest percentage of forested land area. In the divisions, the land types with a relatively low percentage of area are shrublands, wetlands, artificial surfaces, bare land, and permanent snow and ice.

The eight types of land cover in Karen and Mon include cultivated land, forest, grassland, shrub, wetland, water bodies, man-made surfaces, and bare ground. Figs. 11 and 12 illustrate the spatial distribution and area changes of land cover for the periods between 1990 and 2020. In order to identify the primary factors driving the conversion of land cover types, the study calculated the land cover shift matrix using MLC30 products for the two periods, 1990 and 2020, in Karen State and Mon State. Table III presents the results, indicating that significant changes occurred in land cover over the 30-year period. Notably, there was an increase in forest area and a decrease in grassland area, with forest cover expanding by 4049 km^2, and grassland decreasing by 4319 km^2. The increase in forest cover was mainly due to the conversion of grassland (3542 km^2) and cultivated land (1494 km^2). In addition, there was an increase in cultivated land, artificial surfaces, and water bodies, with artificial surfaces showing the largest rate of change at 163.26%, primarily through the conversion of cultivated land, forests, and grasslands. Shrublands and wetlands decreased in area by 555 km^2 and 94 km^2, respectively, mainly from conversion to forest and cultivated land. Overall, land cover conversion in Karen State and Mon State followed a pattern of conversion of cultivated land and

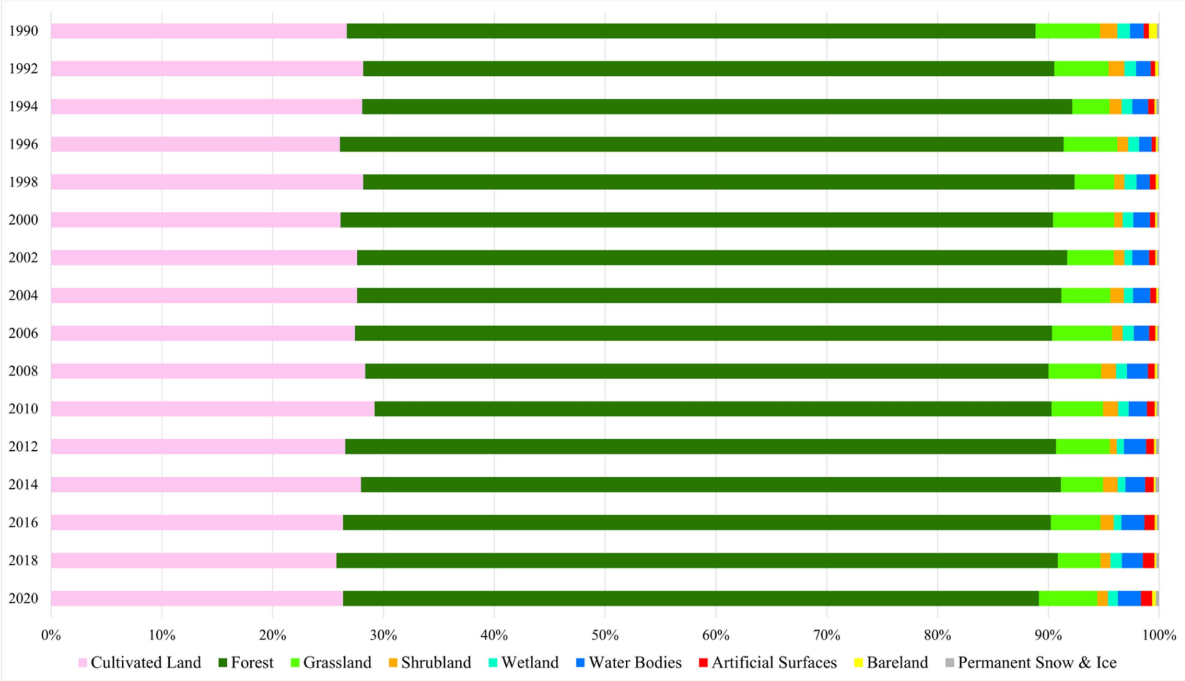

Fig. 10. Changes in different land cover types in Myanmar, 1990–2020.

TABLE II
PERCENTAGE OF MYANMAR'S LAND COVER IN 2020

	Cultivated land	Forest	Grassland	Shrubland	Wetland	Water Bodies	Artificial Surfaces	Bare land	Permanent Snow and Ice	Total Area/(km^2)
Bago	45.68	42.42	4.61	1.49	0.25	3.87	1.61	0.08	0.00	40666
Shan	17.41	71.74	7.66	1.85	0.12	0.55	0.65	0.01	0.00	168323
Tanintharyi	4.05	86.00	0.75	0.00	5.30	3.22	0.67	0.02	0.00	42776
Karen	18.44	76.23	3.49	0.15	0.04	1.06	0.56	0.03	0.00	31554
Kachin	6.17	85.55	2.02	0.40	0.12	1.32	0.54	1.71	2.16	99152
Kayah	18.78	57.80	21.74	0.43	0.08	0.70	0.46	0.01	0.00	12357
Magway	56.99	18.51	16.40	3.85	0.01	2.45	1.24	0.55	0.00	47217
Mandalay	59.64	27.53	6.93	0.61	0.15	1.97	2.70	0.47	0.00	39418
Mon	34.51	58.33	1.92	0.11	0.42	2.61	2.07	0.03	0.00	11476
Chin	1.94	92.28	4.70	0.09	0.01	0.48	0.49	0.00	0.00	40006
Rakhine	17.21	71.63	1.02	0.03	5.60	4.10	0.41	0.00	0.00	37153
Sagaing	33.32	60.00	3.11	0.40	0.08	1.72	1.10	0.26	0.00	105275
Yangon	67.60	15.70	2.12	0.16	1.41	6.26	6.60	0.14	0.00	10081
Ayeyarwady	64.15	20.47	2.03	0.08	3.72	8.27	1.25	0.02	0.00	35173

grassland into forest, conversion of cultivated land, forest, and grassland into artificial surfaces, and conversion of shrublands and wetlands into forest and cultivated land.

Figs. 13 and 14 illustrate the spatial distribution and area changes of land cover in Yangon for the periods between 1990 and 2020. The results indicate significant changes, with an expansion of artificial surfaces in all directions and a continuous decrease in cultivated land. Table IV presents Yangon's land cover transfer matrix from 1990 to 2020, revealing that cultivated land and grassland have decreased significantly by 1113 km^2 and 300 km^2, respectively. Cultivated land was mainly converted to artificial surfaces (523 km^2) and water bodies (322 km^2), while grassland was primarily converted to forest and cultivated land, accounting for 58.7% and 21.3% of the grassland area

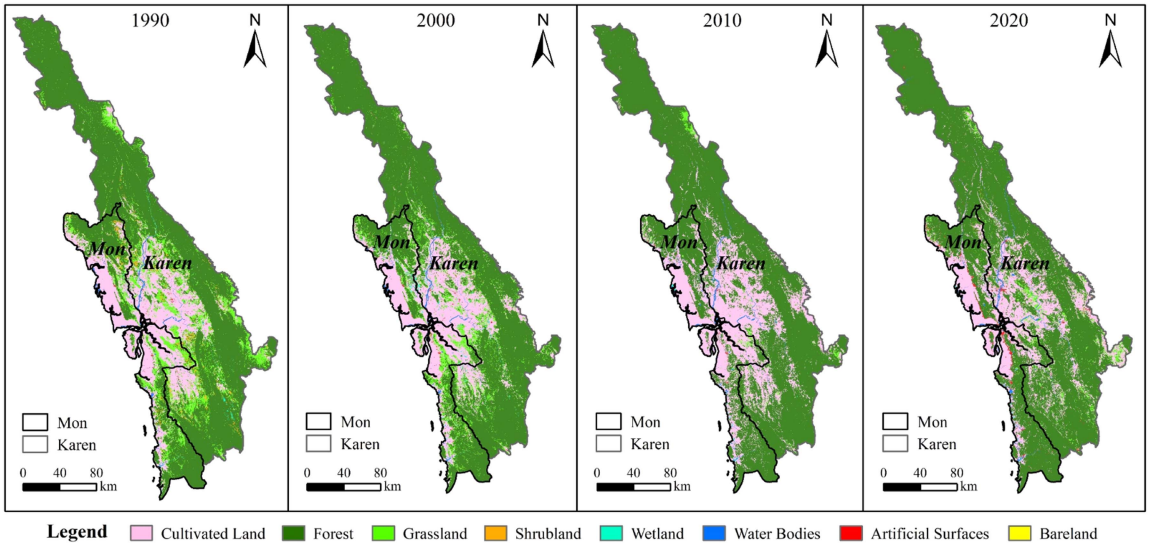

Fig. 11. Land cover classification results for Karen State and Mon State, 1990–2020.

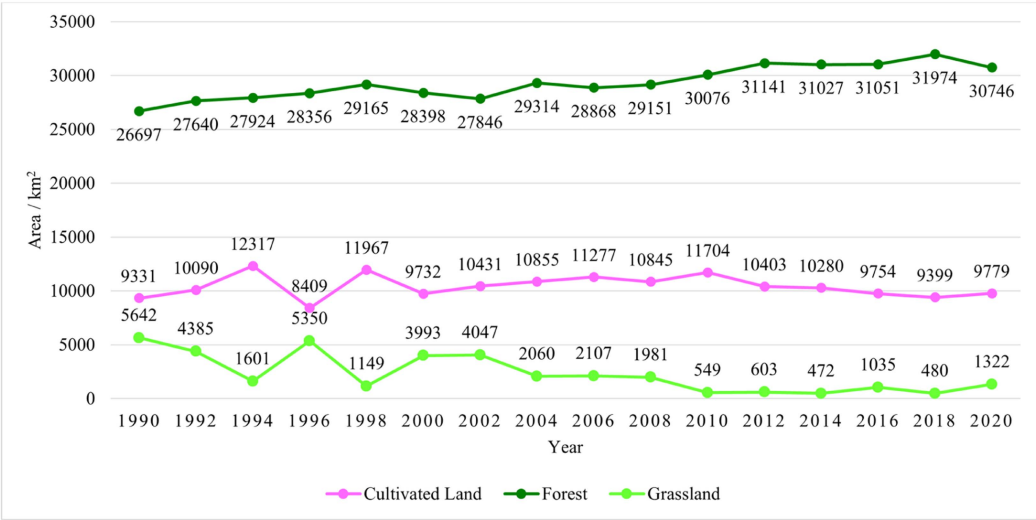

Fig. 12. Change in cultivated land, forest, and grassland in Karen State and Mon State, 1990–2020.

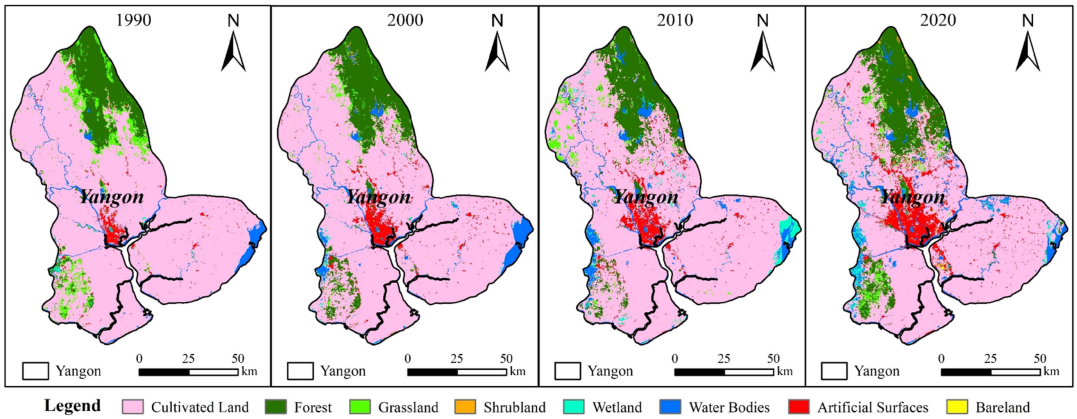

Fig. 13. Land cover classification results for Yangon, 1990–2020.

TABLE III
LAND COVER TRANSFER MATRIX FOR KAREN AND MON STATES, 1990–2020

		2020								
	Class	Cultivated land	Forest	Grassland	Shrubland	Wetland	Water bodies	Artificial surfaces	Bare land	Total
1990	Cultivated land	6993.6	1494.4	459.0	1.3	24.5	156.7	195.7	5.7	9331.0
	Forest	1058.5	25113.6	344.1	37.2	6.2	44.9	90.0	2.3	26696.9
	Grassland	1490.6	3542.2	463.8	9.3	1.0	53.7	77.2	3.7	5641.7
	Shrubland	44.4	505.0	52.8	12.4	0.1	0.6	0.9	0.0	616.1
	Wetland	31.9	67.7	0.8	0.0	12.8	39.9	1.5	0.0	154.5
	Water bodies	85.6	4.0	0.6	0.0	14.1	323.9	2.7	0.3	431.1
	Artificial surfaces	74.7	19.4	1.2	0.0	0.9	14.5	46.7	0.1	157.5
	Bare land	0.0	0.2	0.0	0.0	0.3	0.3	0.0	0.0	0.8
	Total	9779.3	30746.5	1322.4	60.2	59.9	634.5	414.7	12.2	43029.6

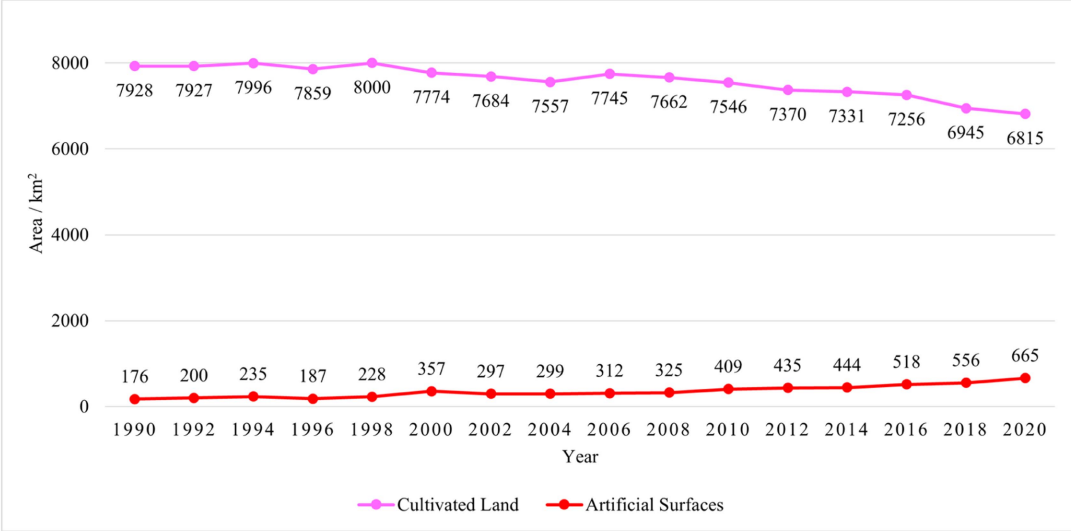

Fig. 14. Change in cultivated land, artificial surface, Yangon, 1990–2020.

TABLE IV
LAND COVER TRANSFER MATRIX, YANGON, 1990–2020

		2020								
	Class	Cultivated land	Forest	Grassland	Shrubland	Wetland	Water bodies	Artificial surfaces	Bare land	Total
1990	Cultivated land	6558.4	268.2	141.6	0.8	100.0	321.9	523.6	13.7	7928.2
	Forest	41.7	982.9	14.1	1.4	12.9	42.1	5.6	0.1	1100.7
	Grassland	109.3	301.9	56.6	13.6	2.3	18.6	11.3	0.5	514.0
	Shrubland	0.5	2.1	0.3	0.0	0.0	0.1	0.0	0.0	2.9
	Wetland	11.2	4.6	0.1	0.0	7.9	9.9	1.2	0.1	35.0
	Water bodies	60.3	10.3	0.6	0.0	17.9	230.2	4.4	0.1	323.8
	Artificial surfaces	33.6	12.5	0.8	0.0	1.0	8.8	119.1	0.1	176.0
	Bare land	0.0	0.0	0.0	0.0	0.0	0.0	0.0	0.0	0.0
	Total	6815.0	1582.4	214.1	15.7	142.1	631.5	665.3	14.6	10080.7

in 1990, respectively. The most significant increases in area were observed for artificial surfaces, forests, wetlands, and water bodies, with cultivated land being the main source of increase in area for artificial surfaces, wetlands, and water bodies. In contrast, the main sources of increase in forest area were grassland and cultivated land. This suggests that land cover conversion in Yangon follows a pattern of cultivated land conversion to artificial surfaces, wetlands, and water bodies, and forest transfer from cultivated land and grassland.

As the most economically developed region in Myanmar, human activities had a significant impact on land cover change in Yangon. Over the past 30 years, there has been a steady decline in cultivated land, an expansion of artificial surfaces, and an increase in forest, wetland, and water bodies. These changes may be attributed to the government's agricultural development policies, the promotion of economic forestry plantations, the implementation of wetland and water body conservation policies, and the push for urbanization and industrialization.

D. Uncertainty Analysis and Prospects

In this study, a long-term land cover classification product was developed for Myanmar using Landsat remote sensing image data. Although the MLC30 product generally performs well, uncertainties still need to be resolved in the analysis as follows.

One uncertainty is the accuracy of the sample points. While high-quality sample points from 2000, 2010, and 2020 were used, hand-selected points from other years were also used, which may increase the uncertainty of the sample points and reduce the classification accuracy. In future studies, it is worthwhile to include more time points and high-quality sample points to cover a wider range of years and improve the reliability of the classification.

Another uncertainty is the issue of time series continuity. Long-term land cover classification products should ensure continuity between time points for effective change analyses. However, differences in remote sensing images and misclassification of different land types may lead to discontinuities in some areas. In future studies, algorithms or methods to achieve time series continuity could be explored to improve the comparability and continuity of classification products.

With the development of remote sensing technology, remote sensing data with higher resolution, more frequency bands, and more time points may be available in future studies. In addition, multisource data fusion can provide more comprehensive land cover information. Future research could focus on improving data quality, classification methods, and data fusion techniques to enhance classification accuracy, time series continuity, and reliability of classification products. This will contribute to a better understanding of potential land cover and change trends and provide more accurate information to support relevant decision-making and conclusion management.

V. Conclusion

This study used the GEE platform and a training sample migration framework to produce an MLC30 dataset of 30 m per two-year period from 1990 to 2020. Long time series of land cover data are essential parameters for exploring environmental change and climate change in Myanmar and are relevant for studying carbon neutrality. Specific findings are presented as follows.

1) The average OA of the MLC30 dataset is 0.83, the Kappa coefficient is 0.79, the specificity is 0.94, and the F1-score is 0.78. Compared with the available 2020 land cover data (i.e., GlobeLand30, FROM-GLC, and Dynamic World), this represents an improvement of 0.07 in OA, 0.08 in Kappa, 0.01 in specificity, and 0.04 in F1-score.
2) There is a clear spatial separation of land cover types in Myanmar. Forests, grasslands, and shrublands are mainly found in the eastern, western, and northern regions. Artificial surfaces and cultivated land are mainly concentrated in the central and southern regions. Wetlands are mainly found in the western and southern coastal areas. Bare land and permanent snow and ice are concentrated in the northern Kachin State.
3) During the 30-year period, Myanmar experienced significant changes in land cover types, with different regions showing different patterns of land cover change. However, there was an overall decrease in the area of cultivated land and an increase in the area of artificial surfaces and forests.

As a possible future research direction, using the MLC30 dataset as baseline data, a more comprehensive perspective on the causes of land cover change occurrence and changes in its vegetation carbon storage can be analyzed and explored to enhance the possibility of achieving carbon neutrality targets and ecologically sustainable development. In the future, we will also explore the dynamic generation of land cover samples using domain-adaptive remote sensing image retrieval methods [44].

Acknowledgment

The authors would like to thank the editors and the anonymous reviewers for their constructive comments and suggestions, which greatly helped improve the quality of the article.

References

[1] L. Zhu, H. Xing, and D. Hou, "Analysis of carbon emissions from land cover change during 2000 to 2020 in Shandong Province, China," *Sci. Rep.*, vol. 12, no. 1, pp. 1–12, 2022.
[2] E. Kosczor, M. Forkel, J. Hernández, D. Kinalczyk, F. Pirotti, and E. Kutchartt, "Assessing land surface phenology in Araucaria-Nothofagus forests in Chile with Landsat 8/Sentinel-2 time series," *Int. J. Appl. Earth Observ. Geo-Inf.*, vol. 112, Jun. 2022, Art. no. 102862.
[3] M. Feng and Y. Bai, "A global land cover map produced through integrating multi-source datasets," *Big Earth Data*, vol. 3, no. 3, pp. 191–219, 2019.
[4] M. C. Hansen, R. S. Defries, J. R. G. Townshend, and R. Sohlberg, "Global land cover classification at 1 km spatial resolution using a classification tree approach," *Int. J. Remote Sens.*, vol. 21, no. 6, pp. 1331–1364, 2000.
[5] T. R. Loveland et al., "Development of a global land cover characteristics database and IGBP DISCover from 1 km AVHRR data," *Int. J. Remote Sens.*, vol. 21, no. 6, pp. 1303–1330, 2000.
[6] J. Yang, Y. He, and J. Caspersen, "Region merging using local spectral angle thresholds: A more accurate method for hybrid segmentation of remote sensing images," *Remote Sens. Environ.*, vol. 190, pp. 137–148, 2017.
[7] D. Sulla-Menashe, J. M. Gray, S. P. Abercrombie, and M. A. Friedl, "Hierarchical mapping of annual global land cover 2001 to present: The MODIS collection 6 land cover product," *Remote Sens. Environ.*, vol. 222, pp. 183–194, Mar. 2019.

[8] M. A. Friedl et al., "MODIS collection 5 global land cover: Algorithm refinements and characterization of new datasets," *Remote Sens. Environ.*, vol. 114, no. 1, pp. 168–182, Jan. 2010.
[9] W. Li et al., "Gross and net land cover changes in the main plant functional types derived from the annual ESA CCI land cover maps (1992–2015)," *Earth Syst. Sci. Data*, vol. 10, pp. 219–234, 2018.
[10] S. Bontemps et al., "Consistent global land cover maps for climate modelling communities: Current achievements of the ESA' land cover CCI," in *Proc. ESA Living Planet Symp.*, 2013, vol. 13, pp. 9–13.
[11] H. Liu, P. Gong, J. Wang, N. Clinton, Y. Bai, and S. Liang, "Annual dynamics of global land cover and its long-term changes from 1982 to 2015," *Earth Syst. Sci. Data*, vol. 12, pp. 1217–1243, 2020.
[12] B. Yang, L. Qin, J. Liu, and X. Liu, "UTRNet: An unsupervised time-distance-guided convolutional recurrent network for change detection in irregularly collected images," *IEEE Trans. Geosci. Remote Sens.*, vol. 60, 2022, Art. no. 4410516.
[13] B. Yang, Y. Mao, L. Liu, X. Liu, Y. Ma, and J. Li, "From trained to untrained: A novel change detection framework using randomly initialized models with spatial–channel augmentation for hyperspectral images," *IEEE Trans. Geosci. Remote Sens.*, vol. 61, 2023, Art. no. 4402214.
[14] J. Chen et al., "Global land cover mapping at 30 m resolution: A POK-based operational approach," *ISPRS J. Photogramm. Remote Sens.*, vol. 103, pp. 7–27, May 2015.
[15] P. Gong et al., "Stable classification with limited sample : Transferring a 30-m resolution sample set collected in 2015 to mapping 10-m resolution global land cover in 2017," *Sci. Bull.*, vol. 64, pp. 370–373, 2019.
[16] P. Gong et al., "Finer resolution observation and monitoring of global land cover : First mapping results with Landsat TM and ETM + data," *Int. J. Remote Sens.*, vol. 34, no. 7, pp. 37–41, 2013.
[17] X. Zhang, L. Liu, X. Chen, Y. Gao, S. Xie, and J. Mi, "GLC_FCS30 : Global land-cover product with fine classification system at 30 m using time-series Landsat imagery," *Earth Syst. Sci. Data*, vol. 13, pp. 2753–2776, 2021.
[18] X. Liu et al., "High-spatiotemporal-resolution mapping of global urban change from 1985 to 2015," *Nature Sustain.*, vol. 3, pp. 564–570, 2020.
[19] C. F. Brown et al., "Dynamic world, near real-time global 10 m land use land cover mapping," *Sci. Data*, vol. 9, no. 1, pp. 1–17, 2022.
[20] G. Z. Xian et al., "Implementation of the CCDC algorithm to produce the LCMAP Collection 1.0 annual land surface change product," *Earth Syst. Sci. Data*, vol. 14, no. 1, pp. 143–162, 2022.
[21] A. Ghorbanian, M. Kakooei, M. Amani, S. Mahdavi, A. Mohammadzadeh, and M. Hasanlou, "Improved land cover map of Iran using Sentinel imagery within Google Earth Engine and a novel automatic workflow for land cover classification using migrated training samples," *ISPRS J. Photogramm. Remote Sens.*, vol. 167, pp. 276–288, 2020.
[22] H. Huang, J. Wang, C. Liu, L. Liang, C. Li, and P. Gong, "The migration of training samples towards dynamic global land cover mapping," *ISPRS J. Photogramm. Remote Sens.*, vol. 161, pp. 27–36, 2020.
[23] A. Poortinga et al., "Mapping plantations in Myanmar by fusing Landsat-8, Sentinel-2 and Sentinel-1 data along with systematic error quantification," *Remote Sens.*, vol. 11, no. 7, pp. 1–19, 2019.
[24] H. Xing et al., "Consistency analysis and accuracy assessment of eight global forest datasets over Myanmar," *Appl. Sci.*, vol. 11, no. 23, 2021, Art. no. 11348.
[25] M. Y. Oo, S. Bonnet, and S. Garivait, "A preliminary assessment of the distribution of vegetation fires in Myanmar and key drivers," *J. Sustain. Energy Environ.*, vol. 10, pp. 85–89, 2019.
[26] J. Li, J. Wang, J. Zhang, J. Zhang, and H. Kong, "Dynamic changes of vegetation coverage in China-Myanmar economic corridor over the past 20 years," *Int. J. Appl. Earth Observ. Geo-Inf.*, vol. 102, 2021, Art. no. 102378.
[27] Y. Jin, A. Li, J. Bian, X. Nan, and G. Lei, "Modeling the impact of investment and national planning policies on future land use development: A case study for Myanmar," *ISPRS Int. J. Geo-Inf.*, vol. 12, no. 1, 2023, Art. no. 22.
[28] P. T. Tun, T. T. Nguyen, and A. Buerkert, "Transformation of agricultural landscapes and its consequences for natural forests in Southern Myanmar within the last 40 years," *Remote Sens.*, vol. 15, no. 6, 2023, Art. no. 1537.
[29] P. Fan et al., "Urbanization, economic development, and environmental changes in transitional economies in the global south: A case of Yangon," *Ecol. Process.*, vol. 11, no. 1, 2022, Art. no. 65.
[30] L. Zhu, X. Jiang, L. Zhao, H. Qu, and W. Sun, "A temporal-spectral value and shape change detection method integrating thematic index information and spectral band information," *Environ. Sci. Pollut. Res.*, vol. 30, no. 16, pp. 47408–47421, 2023.
[31] L. Zhu, H. Xing, L. Zhao, H. Qu, and W. Sun, "A change type determination method based on knowledge of spectral changes in land cover types," *Earth Sci. Inform.*, vol. 16, pp. 1265–1279, 2023.
[32] J. Chen, X. Cao, S. Peng, and H. Ren, "Analysis and applications of GlobeLand30: A review," *ISPRS Int. J. Geo-Inf.*, vol. 6, no. 8, pp. 230–247, 2017.
[33] M. A. Brovelli, M. E. Molinari, E. Hussein, J. Chen, and R. Li, "The first comprehensive accuracy assessment of Globeland 30 at a national level: Methodology and results," *Remote Sens.*, vol. 7, no. 4, pp. 4191–4212, 2015.
[34] H. Xing, L. Zhu, J. Niu, B. Chen, W. Wang, and D. Hou, "A land cover change detection method combing spectral values and class probabilities," *IEEE Access*, vol. 9, pp. 83727–83739, 2021.
[35] H. Xing, L. Zhu, D. Hou, and T. Zhang, "Integrating change magnitude maps of spectrally enhanced multi-features for land cover change detection," *Int. J. Remote Sens.*, vol. 42, no. 11, pp. 4284–4308, 2021.
[36] A. Baraldi and F. Parmiggiani, "Investigation of the textural characteristics associated with gray level cooccurrence matrix statistical parameters," *IEEE Trans. Geosci. Remote Sens.*, vol. 33, no. 2, pp. 293–304, Mar. 1995.
[37] K. Tan, Y. Zhang, X. Wang, and Y. Chen, "Object-based change detection using multiple classifiers and multi-scale uncertainty analysis," *Remote Sens.*, vol. 11, no. 3, pp. 1–17, 2019.
[38] X. Yang et al., "Monthly estimation of the surface water extent in France at a 10-m resolution using Sentinel-2 data," *Remote Sens. Environ.*, vol. 244, 2020, Art. no. 111803.
[39] M. Amani et al., "Google Earth Engine cloud computing platform for remote sensing big data applications: A comprehensive review," *IEEE J. Sel. Topics Appl. Earth Observ. Remote Sens.*, vol. 13, pp. 5326–5350, 2020.
[40] Y. Tu, B. Chen, T. Zhang, and B. Xu, "Regional mapping of essential urban land use categories in China: A segmentation-based approach," *Remote Sens.*, vol. 12, no. 7, 2020, Art. no. 1058.
[41] W. Y. Yan, K. van Ewijk, P. Treitz, and A. Shaker, "Effects of radiometric correction on cover type and spatial resolution for modeling plot level forest attributes using multispectral airborne LiDAR data," *ISPRS J. Photogramm. Remote Sens.*, vol. 169, no. 9, pp. 152–165, 2020.
[42] S. O. Los, F. A. Street-Perrott, N. J. Loader, and C. A. Froyd, "Detection of signals linked to climate change, land-cover change and climate oscillators in tropical montane cloud forests," *Remote Sens. Environ.*, vol. 260, 2021, Art. no. 112431.
[43] T. Sakamoto, "Incorporating environmental variables into a MODIS-based crop yield estimation method for United States corn and soybeans through the use of a random forest regression algorithm," *ISPRS J. Photogramm. Remote Sens.*, vol. 160, pp. 208–228, 2020.
[44] S. Wang, D. Hou, and H. Xing, "A self-supervised-driven open-set unsupervised domain adaptation method for optical remote sensing image scene classification and retrieval," *IEEE Trans. Geosci. Remote Sens.*, vol. 61, 2023, Art. no. 5605515.

Huaqiao Xing received the Ph.D. degree in geographic information systems from the China University of Mining and Technology, Beijing, China, in 2017.

He is currently an Associate Professor with the School of Surveying and Geo-Informatics, Shandong Jianzhu University, Jinan, China. His main research interests include land cover change detection, geospatial web service, and remote sensing image retrieval.

Linye Zhu was born in Wuyishan City, Fujian Province, China, in 1997. She received the master's degree in surveying and mapping science and technology from Shandong Jianzhu University, Jinan, China, in 2022. She is currently working toward the Ph.D. degree in surveying and mapping science and technology with the China University of Mining and Technology, Beijing, China.

Her main research interest focuses on land cover change detection.

Yuqing Zhang was born in Linyi, China, in 2000. She received the bachelor's degree in geospatial information engineering from Linyi University, Linyi, China, in 2022. She is currently working toward the master's degree in surveying and mapping science and technology with Shandong Jianzhu University, Jinan, China.

Her main research interest focuses on land cover sample migration.

Dongyang Hou (Member, IEEE) received the Ph.D. degree in geographic information systems from the China University of Mining and Technology, Xuzhou, China, in 2016.

He is currently an Associate Professor with the School of Geosciences and Info-Physics, Central South University, Changsha, China. His main research interests include spatial–temporal data crawling, mining, and remote sensing image retrieval.

Cansong Li was born in 1980. He received the Ph.D. degree in human geography from Beijing Normal University, Beijing, China, in 2020.

He is currently a Professor with the Faculty of Geography, Yunnan Normal University, Kunming, China. His research interests mainly include the application of GIS in social sciences.